PHYSICAL REVIEW D **80,** 073005 (2009)

Short-baseline electron neutrino disappearance at a neutrino factory

Carlo Giunti,[1,*] Marco Laveder,[2,†] and Walter Winter[3,‡]

[1]*INFN, Sezione di Torino, Via P. Giuria 1, I-10125 Torino, Italy*

[2]*Dipartimento di Fisica "G. Galilei," Università di Padova and INFN, Sezione di Padova, Via F. Marzolo 8, I-35131 Padova, Italy*

[3]*Institut für Theoretische Physik und Astrophysik, Universität Würzburg, D-97074 Würzburg, Germany*

(Received 1 August 2009; published 13 October 2009)

We discuss short-baseline and very-short-baseline ν_e disappearance at a neutrino factory. We take into account geometric effects, such as from averaging over the decay straights, and the uncertainties of the cross sections. We follow an approach similar to reactor experiments with two detectors: we use two sets of near detectors at different distances to cancel systematics. We demonstrate that such a setup is very robust with respect to systematics, and can have excellent sensitivities to the effective mixing angle and squared-mass splitting. In addition, we allow for *CPT* invariance violation, which can be tested (depending on the parameters) up to a 0.1% level.

DOI: 10.1103/PhysRevD.80.073005 PACS numbers: 14.60.Pq

I. INTRODUCTION

Neutrino oscillation experiments have shown that neutrinos are massive particles with at least two squared-mass differences: $\Delta m^2_{\mathrm{SOL}} \simeq 8 \times 10^{-5}\ \mathrm{eV}^2$, measured in solar and very-long-baseline reactor neutrino experiments, and $\Delta m^2_{\mathrm{ATM}} \simeq 2 \times 10^{-3}\ \mathrm{eV}^2$, measured in atmospheric and long-baseline neutrino experiments (see Refs. [1–10]). These two Δm^2's are perfectly accommodated in the framework of three-neutrino mixing, where there are two independent squared-mass differences. However, there are experimental anomalies which may indicate the existence of short-baseline (SBL) or very-short-baseline (VSBL) oscillations generated by a third Δm^2 which is much larger than the other two: $\Delta m^2_{\mathrm{SBL}} \gtrsim 10^{-1}\ \mathrm{eV}^2$ or $\Delta m^2_{\mathrm{VSBL}} \gtrsim 10\ \mathrm{eV}^2$. Among these anomalies, the most well known is the LSND signal in favor of SBL $\bar{\nu}_\mu \to \bar{\nu}_e$ oscillations [11], which has not been confirmed by other experiments and is currently disfavored by the negative results of KARMEN [12] and MiniBooNE [13]. Less well known are the Gallium radioactive source experiments anomaly [14] and the MiniBooNE low-energy anomaly [13], which could be explained by SBL [15,16] or VSBL [17,18] ν_e disappearance.

The existence of a third Δm^2 requires the existence of at least a fourth massive neutrino which corresponds, in the flavor basis, to the existence of a sterile neutrino ν_s, i.e., a fermion which is a singlet under the standard model symmetries. Hence it is electrically neutral and does not take part in weak interactions. If the three active neutrinos ν_e, ν_μ, and ν_τ are mixed with the sterile neutrino, neutrino oscillation experiments can observe the disappearance of active neutrinos into ν_s.

In light of the above-mentioned anomalies, it is interesting to investigate the possibility of (V)SBL ν_e disappearance with future high-precision experiments. In general, it is important to investigate the possibility of ν_e disappearance generated by a Δm^2 different from $\Delta m^2_{\mathrm{SOL}}$ and $\Delta m^2_{\mathrm{ATM}}$ in order to constrain schemes with mixing of four (see Refs. [1,4,6,8]) or more [19,20] massive neutrinos. These schemes have been studied mostly in connection with the LSND anomaly, but the latest global fits of the experimental data, including the LSND signal, are not good [4,8]. However, the schemes with mixing of more than three neutrinos may be realized in nature independently of the LSND signal. Hence, it is important to investigate the phenomenology of sterile neutrinos with an open mind, not only through neutrino oscillations [21–29], but also by studying their effects in astrophysics [30–35] and cosmology [36–38].

If there is (V)SBL electron neutrino disappearance, it must be mainly into sterile neutrinos, because the mixing of the three active neutrinos with the fourth massive neutrino must be small in order to fit the data on $\nu_e \to \nu_{\mu,\tau}$ oscillations generated by $\Delta m^2_{\mathrm{SOL}}$ and the data on $\nu_\mu \to \nu_\tau$ oscillations generated by $\Delta m^2_{\mathrm{ATM}}$. In the $3+1$ four-neutrino schemes (see Refs. [1,4,6,8]) with $\Delta m^2_{(\mathrm{V})\mathrm{SBL}} = |\Delta m^2_{41}| \gg \Delta m^2_{\mathrm{ATM}} = |\Delta m^2_{31}| \gg \Delta m^2_{\mathrm{SOL}} = |\Delta m^2_{21}|$, where $\Delta m^2_{kj} \equiv m^2_k - m^2_j$, the mixing matrix U must be such that $|U_{e4}|, |U_{\mu 4}|, |U_{\tau 4}| \ll 1$ and $|U_{s4}| \simeq 1$. Therefore, the amplitudes of the (V)SBL oscillation channels, $A_{\alpha\beta} = 4|U_{\alpha 4}|^2 |U_{\beta 4}|^2$ for $\alpha \neq \beta$, are such that $A_{ab} \ll A_{as}$ for $a, b = e, \mu, \tau$.

In this paper we study the sensitivity of neutrino factory experiments to (V)SBL ν_e and $\bar{\nu}_e$ disappearance, which in practice has been investigated so far mainly through SBL reactor neutrino experiments ($\bar{\nu}_e$ disappearance).

We will first study, in Sec. IV, (V)SBL ν_e and $\bar{\nu}_e$ disappearance at a neutrino factory assuming exact *CPT*

*giunti@to.infn.it
†laveder@pd.infn.it
‡winter@physik.uni-wuerzburg.de

symmetry, which implies $P_{ee} = P_{\bar{e}\bar{e}}$ (see Ref. [7]), considering the simplest case of effective two-neutrino mixing with

$$P_{ee} = P_{\bar{e}\bar{e}} = 1 - \sin^2(2\theta)\sin^2\left(\frac{\Delta m^2 L}{4E}\right), \tag{1}$$

where, from now on, $\Delta m^2 = \Delta m^2_{(\mathrm{V})\mathrm{SBL}}$. This is the case of four-neutrino mixing schemes with $\Delta m^2 = |\Delta m^2_{41}| \gg \Delta m^2_{\mathrm{ATM}} = |\Delta m^2_{31}| \gg \Delta m^2_{\mathrm{SOL}} = |\Delta m^2_{21}|$. In the $3+1$ schemes, the amplitude of the oscillations is related to the U_{e4} element of the mixing matrix by $\sin^2(2\theta) = 4|U_{e4}|^2(1 - |U_{e4}|^2)$ (see Refs. [1,4,6,8]).

The *CPT* symmetry is widely believed to be exact, because it is a fundamental symmetry of local relativistic quantum field theory (see Ref. [39]). However, in recent years studies of extensions of the standard model have shown that it is possible to have violations of the Lorentz and *CPT* symmetries (see Refs. [40–42]), and several phenomenological studies of neutrino oscillations with different masses and mixing for neutrinos and antineutrinos appeared in the literature [43–54]. We will consider this scenario in the simplest case of effective two-neutrino mixing with

$$P_{ee} = 1 - \sin^2(2\theta_\nu)\sin^2\left(\frac{\Delta m^2_\nu L}{4E}\right), \tag{2}$$

$$P_{\bar{e}\bar{e}} = 1 - \sin^2(2\theta_{\bar{\nu}})\sin^2\left(\frac{\Delta m^2_{\bar{\nu}} L}{4E}\right). \tag{3}$$

This kind of *CPT* violation in a four-neutrino mixing scheme could reconcile the LSND signal with the other neutrino oscillation data [50] and/or could explain the Gallium radioactive source experiments anomaly and the MiniBooNE low-energy anomaly together with the absence of $\bar{\nu}_e$ disappearance in reactor neutrino experiments [18]. Let us emphasize that the reconciliation of the LSND anomaly with the results of other neutrino oscillation experiments is not possible in three-neutrino mixing schemes even if *CPT* violation is allowed [8,52].

Another hint in favor of a possible *CPT* violation comes from the recent measurement of ν_μ and $\bar{\nu}_\mu$ disappearance in the MINOS experiment [55], which indicates different best-fit values of the oscillation parameters of ν_μ and $\bar{\nu}_\mu$: $\Delta\bar{m}^2_{\mathrm{MINOS}} \simeq 2 \times 10^{-2}$ eV^2 and $\sin^2\bar{\theta}_{\mathrm{MINOS}} \simeq 0.6$ for $\bar{\nu}_\mu$'s, whereas $\Delta m^2_{\mathrm{MINOS}} \simeq 2.4 \times 10^{-3}$ eV^2 and $\sin^2\theta_{\mathrm{MINOS}} \simeq 1$ for ν_μ's. The best-fit values and allowed region of the ν_μ oscillation parameters are in agreement with atmospheric $\nu_\mu \to \nu_\tau$ oscillations. Since the 90% C.L. allowed region of the $\bar{\nu}_\mu$ oscillation parameters has a marginal overlap with the much smaller 90% C.L. of the ν_μ oscillation parameters (see the figure on page 11 of Ref. [55]), the MINOS hint in favor of *CPT* violation is rather speculative. Nevertheless, it is interesting to notice that a global separate analysis of neutrino and antineutrino data in the framework of three-neutrino mixing with *CPT* violation leads to different best-fit values of the oscillation parameters of neutrinos and antineutrinos with $\Delta\bar{m}^2_{\mathrm{ATM}} \simeq \Delta\bar{m}^2_{\mathrm{MINOS}}$ and $\sin^2\bar{\theta}_{\mathrm{ATM}} \simeq \sin^2\bar{\theta}_{\mathrm{MINOS}}$, whereas $\Delta m^2_{\mathrm{ATM}} \simeq \Delta m^2_{\mathrm{MINOS}}$ and $\sin^2\theta_{\mathrm{ATM}} \simeq \sin^2\theta_{\mathrm{MINOS}}$ [56]. However, in this paper we do not consider the MINOS hint in favor of *CPT* violation. We concentrate our study on possible *CPT* violations in (V)SBL ν_e and $\bar{\nu}_e$ disappearance due to squared-mass differences larger than about 0.1 eV^2.

Besides those in Eqs. (2) and (3), it is possible to consider other, more complicated, expressions for P_{ee} and $P_{\bar{e}\bar{e}}$, with additional energy-dependent terms in the oscillation phases which could be generated by modified dispersion relations that are different for neutrinos and antineutrinos (see, for example, Refs. [57–62]). However, the introduction of more unknown parameters would make the analysis too cumbersome, without much additional information on the potentiality of a neutrino factory experiment to test *CPT* invariance. In fact, it is plausible that the additional energy-dependent terms in the oscillation phases generate spectral distortions which would make the identification of new physics even easier than in the simplest case that we consider.

In order to test *CPT* invariance (or *small* deviations from it) explicitly, it is convenient to define the averaged neutrino oscillation parameters

$$\theta \equiv \tfrac{1}{2}(\theta_\nu + \theta_{\bar{\nu}}), \qquad \Delta m^2 \equiv \tfrac{1}{2}(\Delta m^2_\nu + \Delta m^2_{\bar{\nu}}), \tag{4}$$

together with the *CPT* asymmetries

$$a_{CPT} \equiv \frac{\theta_\nu - \theta_{\bar{\nu}}}{\theta_\nu + \theta_{\bar{\nu}}}, \qquad m_{CPT} \equiv \frac{\Delta m^2_\nu - \Delta m^2_{\bar{\nu}}}{\Delta m^2_\nu + \Delta m^2_{\bar{\nu}}}, \tag{5}$$

which are constrained in the range between -1 and 1. Then we have

$$\theta_\nu = (1 + a_{CPT})\theta, \tag{6}$$

$$\theta_{\bar{\nu}} = (1 - a_{CPT})\theta, \tag{7}$$

$$\Delta m^2_\nu = (1 + m_{CPT})\Delta m^2, \tag{8}$$

$$\Delta m^2_{\bar{\nu}} = (1 - m_{CPT})\Delta m^2. \tag{9}$$

The limit of *CPT* invariance [Eq. (1)] corresponds to $a_{CPT} = m_{CPT} = 0$. In Sec. V we discuss the potentiality of neutrino factory experiments to discover $a_{CPT} \neq 0$ and/or $m_{CPT} \neq 0$.

The plan of the paper is as follows: in Sec. II we define an "ideal detector" for the measurement of (V)SBL ν_e and $\bar{\nu}_e$ disappearance at a neutrino factory, and we describe our treatment of geometric effects; in Sec. III we discuss the requirements for systematics; in Sec. IV we discuss the sensitivity to (V)SBL ν_e and $\bar{\nu}_e$ disappearance assuming *CPT* invariance, with the survival probability in Eq. (1); in Sec. V we discuss the sensitivity to *CPT* violation consid-

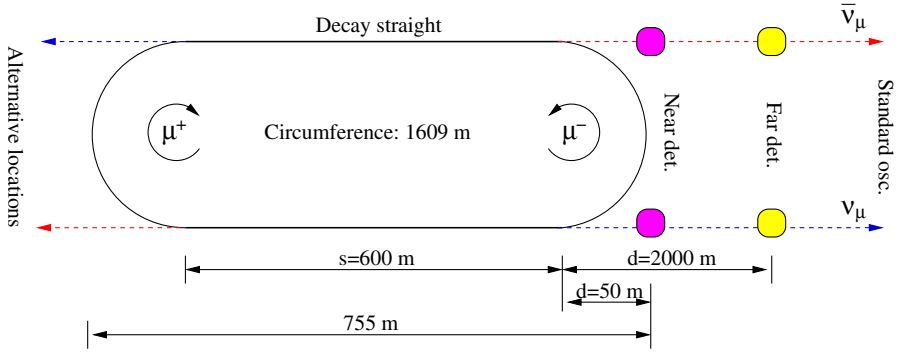

FIG. 1 (color online). Geometry of the decay ring (not to scale). Two possible detector locations are shown at $d = 50$ m and $d = 2000$ m, where d is the distance to the end of the decay straight. The baseline L is the distance between the production point and the detector.

ering the survival probabilities in Eqs. (2) and (3); conclusions are presented in Sec. VI.

II. IDEAL DETECTOR AND GEOMETRIC EFFECTS

Our neutrino factory geometry is based on the International Design Study for the Neutrino Factory baseline setup [63], with the geometry illustrated in Fig. 1. We consider 2.5×10^{20} useful muon decays per polarity and year, with muon energy $E_\mu = 25$ GeV. For the total running time, we consider ten years.

In order to test SBL ν_e disappearance, we add detectors in front of the decay straights as illustrated in Fig. 1. Here ''near'' and ''far'' detectors refer to SBL ν_e disappearance only, whereas the detectors for standard oscillations are much farther away and not relevant for our problem. The straight sections are anticipated to be about $s = 600$ m long. The distance d is the distance between the end of the decay straight and the near detector. The baseline L is the distance between the production point and the near detector, i.e., $d \leq L \leq d + s$. Since the μ^+ and μ^- are assumed to circulate in different directions in the ring, we need pairs of detectors in front of the straights because we want to test CPT invariance.[1]

Since there are no specifications for near detectors at a neutrino factory yet (see Ref. [64] for a generic discussion), we turn the argument around and formulate the requirements for the detectors for this measurement. Our detectors are assumed to measure the total charged current rates with a 100% detection efficiency; a lower efficiency will simply lead to a rescaling of statistics and can be easily compensated by a larger detector mass. The energy threshold is chosen to be 500 MeV, similar to a totally active scintillator detector or an iron calorimeter, and the energy resolution is taken as

$$\Delta E = \varepsilon \sqrt{\frac{E}{E_0}}, \tag{10}$$

with $\varepsilon = 0.55$ GeV and $E_0 = 1$ GeV, which is a conservative estimate for a magnetized iron calorimeter [63]. Similarly, we assume that the neutral current level can be controlled at the level of 10^{-3} from all neutrinos in the beam (see, e.g., Refs. [65,66] in the context of a low-energy neutrino factory). However, we have tested that the results do not strongly depend on these three quantities. We require an excellent flavor identification (at the level of 10^{-3} for the misidentification, as we will see later). Charge identification is also desirable in order to reduce the contamination of the ν_e (or $\bar{\nu}_e$) signal by $\bar{\nu}_e$ (or ν_e) generated by possible (V)SBL $\bar{\nu}_\mu \rightarrow \bar{\nu}_e$ (or $\nu_\mu \rightarrow \nu_e$) oscillations. However, we do not consider the backgrounds from charge misidentification explicitly.[2] For the binning, we use 17 bins between 0.5 and 25 GeV with a bin size of 0.5 GeV (1 bin)—1 GeV (9 bins)—2 GeV (5 bins)—2.5 GeV (2 bins). As the main obstacles for the physics potential, we have identified the extension of the decay straights and the impact of systematics. We discuss the first issue below, and the second issue in the next section. Thereby, we define our ''ideal detectors'' as detectors with the above properties, but no backgrounds or systematics.

Our geometric treatment of the near detectors is based on Ref. [67], which discusses the flux at near detectors in detail. Here we start from the differential event rate from a point source $dN_{\rm PS}/dE$ without oscillations. Taking into account the extension of the straight and the geometry of the detector, the averaged differential event rate is given by[3]

[1]Without a CPT invariance test, detectors in front of one straight are sufficient. The detectors in front of the other straight only increase statistics then.

[2]The level of contamination depends on the oscillation model. Even for large mixing angles driving these oscillations of the potential background, a charge misidentification level of about 10^{-3} would be sufficient.

[3]Note that as a peculiarity compared to Ref. [67], $dN_{\rm PS}/dE$ uses the unoscillated event rate, because the oscillation probability has to be integrated over.

$$\frac{dN_{\rm avg}}{dE} = \frac{1}{s}\int_d^{d+s}\frac{dN}{dE}dL = \frac{1}{s}\int_d^{d+s}\frac{dN_{\rm PS}(L,E)}{dE}\varepsilon(L,E)P_{ee}(L,E)dL. \quad (11)$$

Here $\varepsilon(L,E) = A_{\rm eff}/A_{\rm Det}$ parametrizes the integration over the detector geometry for a fixed baseline L and a given energy E ($A_{\rm Det}$ is the surface area of the detector and $A_{\rm eff}$ is the effective surface area which takes into account the angular dependence of the neutrino flux). Since $dN_{\rm PS}/dE \propto 1/L^2$, we can rewrite this as

$$\frac{dN_{\rm avg}}{dE} = \frac{dN_{\rm PS}(L_{\rm eff},E)}{dE}\frac{L_{\rm eff}^2}{s}\int_d^{d+s}\frac{\varepsilon(L,E)}{L^2}P_{ee}(L,E)dL = \frac{dN_{\rm PS}(L_{\rm eff},E)}{dE}\hat{P}(E), \quad (12)$$

with the average efficiency ratio times probability[4]

$$\hat{P}(E) \equiv \frac{L_{\rm eff}^2}{s}\int_d^{d+s}\frac{\varepsilon(L,E)}{L^2}P_{ee}(L,E)dL, \quad (13)$$

and the effective baseline

$$L_{\rm eff} = \sqrt{d(d+s)}, \quad (14)$$

such that $\hat{P}(E) = 1$ for $\epsilon(L,E) \equiv P_{ee}(L,E) \equiv 1$. We assume $\epsilon(L,E) \equiv 1$ (far distance approximation), which, to a good approximation, is satisfied for ND4 of Ref. [67] (see Fig. 4 therein) for $d \gtrsim 50$ m. This detector is very small (200 kg), but it has a sufficient event rate. At a neutrino factory, the active volume of near detectors is probably going to be rather small, because high granularity and good track reconstruction will be more important than the active volume size [64]. Our ''ideal'' test detectors therefore have 200 kg fiducial volume at very short distances. One can, for longer baselines, upscale the detector mass as

$$m_{\rm Det} \simeq \frac{d\times(d+600\ {\rm m})}{50\ {\rm m}\times 650\ {\rm m}}0.2\ {\rm t} \quad (15)$$

without strong geometric effects from the effective area of the detector (i.e., one still operates in the far distance limit). However, one may choose a different technology for these larger detectors.

For our simulation, we use the GLOBES software [68,69]. We define the exclusion limit as a function of $\sin^2 2\theta$ and Δm^2 as the excluded region obtained in a χ^2 analysis assuming a vanishing true value of θ (i.e., no oscillations). In Fig. 2, we show this exclusion limit for several near detector distances including the effects of averaging over the decay straight (dashed curves) and without averaging (solid curves). This figure is based on our ideal detectors, without taking into account systematics yet. Obviously, the optimal detector locations depend on the region of sensitivity of Δm^2 which is of interest: the smaller Δm^2, the longer the baseline. For instance, for $\Delta m^2 \simeq 1\ {\rm eV}^2$, the best sensitivity is obtained for $d \simeq 20$ km, whereas for $\Delta m^2 \simeq 100\ {\rm eV}^2$, a distance of the order $d = 100$ m is optimal. For short distances d up to a few hundred meters, there is clearly an effect of the averaging over the decay straight. However, note that because of the $1/L^2$ weighting in Eq. (12), the effect becomes negligible for $d \gtrsim 1$ km. Compared to a classical beam dump experiment, one cannot get arbitrarily close to the source without losing information. In the next section, we will discuss the requirements for systematics.

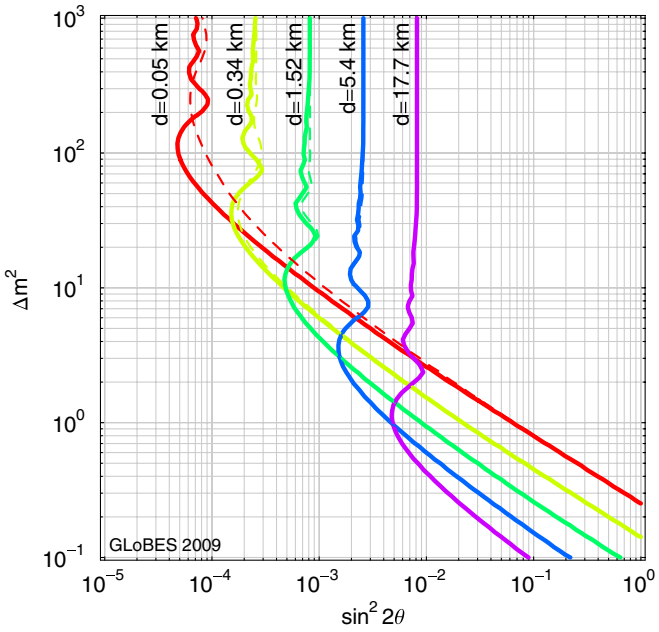

FIG. 2 (color online). Exclusion limit for several near detector distances d and our ideal near detectors (*CPT* invariance assumed; 90% C.L., 2 d.o.f.; two near detectors in front of straights). The dashed curves illustrate the effect of including the averaging over the decay straight, whereas the solid curves are without this averaging. The fiducial detector masses are fixed to 200 kg. Note that there are no systematics included in this figure.

We have also tested a low-energy neutrino factory for this measurement, with similar success. However, in the absence of official numbers for the storage ring geometry and systematics, we will not discuss it in greater detail. In addition, note that the absolute performance is not *a priori* better than for a higher-energy neutrino factory. For instance, assume that the distance d is fixed for geometric reasons. Then the oscillation effect is, to a first approximation, proportional to $1/E^2$ (with E the peak energy of the spectrum), but the statistics roughly increases as E^3 (E^2 from the beam collimation and E from the cross sections),

[4]Note that Eq. (12) implies that in GLOBES a point source spectrum at the effective baseline $L_{\rm eff}$ can be used, which has to be corrected by Eq. (13). We perform Eq. (13) directly in the probability engine.

which means that the net effect is proportional to E_μ. We observed this behavior in our simulation.

III. REQUIREMENTS FOR SYSTEMATICS

As far as systematics is concerned, it is well known from reactor experiments, such as Double Chooz [70] and Daya-Bay [71], that electron neutrino disappearance is most affected by the signal normalization uncertainty (see, e.g., Refs. [72,73]). We expect the same for our measurement. However, compared to reactor experiments, our signal normalization error does not mainly come from the knowledge on the flux, which we may know to the level of 0.1% using various mean monitoring devices [64], but from the knowledge of the cross sections. Because our neutrino energies span the cross section regimes from quasielastic scattering, over resonant pion production, to deep inelastic scattering, it is not *a priori* simple to estimate the accuracy of the knowledge of the cross sections at the time of the measurement. For reactor experiments, on the other hand, the inverse beta decay cross sections are well known. Note that Ref. [29] also uses this well-understood detection reaction for a low-gamma beta beam, whereas we will use a completely orthogonal strategy.

Let us, first of all, illustrate what the main requirements for systematics are. As indicated above, we have tested in Fig. 3 the impact of a signal normalization error and an additional tilt error (tilting the shape of the spectrum). Although the errors are assumed to be rather optimistic (2.5%), there is a significant impact on the sensitivities at all baselines, as we expected. Off the oscillation maxima, as visible in the right panel at large values of Δm^2 where $P_{ee} \simeq 0.5 \sin^2 2\theta$, the signal normalization error σ_{Norm} directly limits the sensitivity to $\sin^2 2\theta \simeq 2\sqrt{2.3}\sigma_{\mathrm{Norm}} \simeq 0.076$ at 1σ (2.3 is the $\Delta\chi^2$ corresponding to 1σ for 2 degrees of freedom). The tilt error tilts the spectrum linearly, and is a first order approximation for a shape error. It is especially important when the spectral information leads to a good sensitivity, in particular, for the shorter baselines (left panel). However, note that this (linear) tilt error cannot fully take into account the uncertainties in the cross sections, because the actual deviation may be nonlinear. We have also tested the impact of backgrounds, energy resolution, and energy threshold. The most important of these three systematics is the background, where the sensitivity is basically limited by the product of background level and background uncertainty. Even for large uncertainties of the background, such as 20%, this product limits the sensitivity to about $0.001 \times 20\% \simeq 10^{-4}$, which is beyond our expectations in the presence of a normalization uncertainty.

In summary, the signal normalization and shape have to be either very well known, or very well measured. The first requirement means that one needs very refined theoretical models for the cross sections; the second possibility means that one needs to measure the cross sections very well. We follow the second approach by considering a setup with two sets of detectors (cf. Fig. 1):

(1) Near detectors at $d = 50$ m with $m_{\mathrm{Det}} = 200$ kg.
(2) Far detectors at $d = 2000$ m with $m_{\mathrm{Det}} = 32$ t.

The signal measured with the near detectors fixes the normalization and shape of the unoscillated signal (for small enough Δm^2). The far detectors are upscaled versions of the near detectors following Eq. (15), which means that geometric effects are almost negligible. The near detectors have optimal sensitivity at a few hundred eV^2 (VSBL), whereas the far detectors have optimal sensitivity at a few eV^2 (SBL). Note that longer baselines may be even better for the far detectors, but then the depth difference between the storage ring and the detectors may become unrealistically large. On the other hand, for distances much

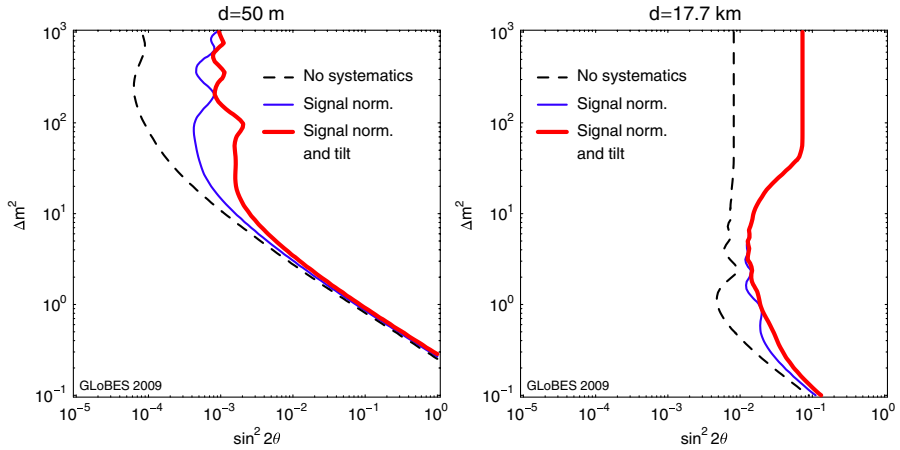

FIG. 3 (color online). The effect of different (hypothetical) systematical errors: A signal normalization error of 2.5% and an additional spectral tilt error of 2.5% have been applied to the exclusion limit for two different detector distances d (90% C.L., 2 d.o.f.). The dashed curves refer to our ideal detectors; the solid curves include systematics. Here the fiducial mass is fixed to 200 kg; the effect of averaging over the decay straight is taken into account. Here CPT invariance is assumed.

shorter than 2 km, one significantly loses sensitivity for small Δm^2.

For systematics, we adopt the most conservative point of view; i.e., we assume that we hardly know anything about the cross sections, neither the normalization nor the shape, but that the cross sections are fully correlated among all detectors measuring the cross sections. Such an error is often called the ''shape error'' and is uncorrelated among all bins. In summary, we include the following systematical errors, similar to the reactor experiments in Ref. [73], and we have tested their impact (we have switched off systematical errors to test their impact):

Shape errors.—uncorrelated among bins and ν-$\bar{\nu}$, but fully correlated among the detectors. These errors include cross section errors, scintillator or detector material properties, etc. In addition, flux errors can be included here (the detectors only measure the product of flux and cross section for the disappearance channel). We estimate this error to be 10%. However, even a larger error does not matter if both near and far detectors are present, but only errors considerably smaller than 10^{-3} improve the result significantly (which is absolutely unrealistic for this type of systematics).

Normalization errors.—uncorrelated between the near and far detectors. These relative normalization errors come from the knowledge on fiducial mass, detector normalization, and analysis cuts (uncorrelated between the detectors). They are typically small if similar detectors are used. For reactor experiments (Double Chooz [70]), this error is about 0.6%, which we use as an estimate. We have tested that there is little dependence on this error unless it can be reduced to the level of 10^{-4} (then there is a small improvement), if the other systematics is present.

Energy calibration errors.—uncorrelated between the near and far detectors of the order 0.5% (similar to the reactor experiments). As we have tested, they are of secondary importance if all the other systematics are present.

Backgrounds.—at the level of 10^{-3} from neutral current events etc., known to the level of 20% (a somewhat conservative estimate from a neutrino factory). If all the other errors are present, backgrounds hardly matter.

The effect of electron neutrino disappearance on the event rates of the individual bins is illustrated in Fig. 4 for the near (left panel) and far (right panel) detectors for several values of Δm^2. For relatively small $\Delta m^2 \sim 1$ eV^2 (diamond curves), the near-far combination will perform similar to the reactor experiments with two detectors, where the near detector measures the shape and the far detector the oscillation effect. For $\Delta m^2 \gg 1000$ eV^2 (cf. triangle curves for comparison), the oscillations average out in both detectors, and $\sin^2 2\theta$ can only be constrained to the level of the shape errors (whereas Δm^2 cannot be measured). For $\Delta m^2 \sim 100$ eV^2 (box curves), the oscillation effect will mainly take place in the near detector, whereas the far detector measures the shape (after averaging). For $\Delta m^2 \sim 10$ eV^2 (star curves), the situation is the most complicated: there are oscillation effects in both detectors, which can lead to intricate parameter correlations.

IV. RESULTS FOR *CPT* INVARIANCE

All results presented in this section are based on our two-baseline setup without a refined systematics treatment, assuming *CPT* invariance, i.e., the equal electron neutrino and antineutrino survival probabilities in Eq. (1).

Figure 5 shows the performance of our near-far model (thick curve), where the effect of using only one set of detectors (near or far) is shown separately as thin curves. If only one set of detectors is used, the result will be limited by the 10% shape errors; i.e., it depends on the assumptions used. However, if the two sets of detectors are used, the impact of systematics cancels and the result is very robust with respect to the assumptions. From the above discus-

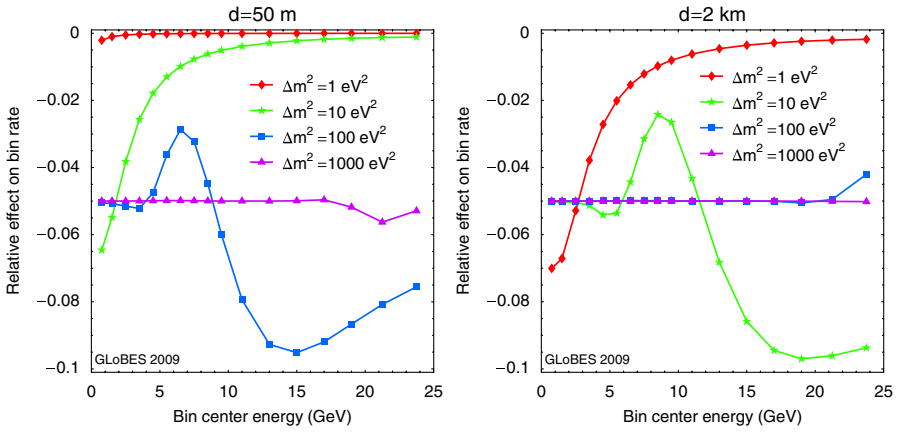

FIG. 4 (color online). Relative effect on the binned (neutrino) event rates for several values of Δm^2, and $\sin^2 2\theta = 0.1$, in the near (left panel) and far (right panel) detectors. For each energy bin we plotted $(R - R_0)/R_0$, where R and R_0 are the expected rates with and without oscillations.

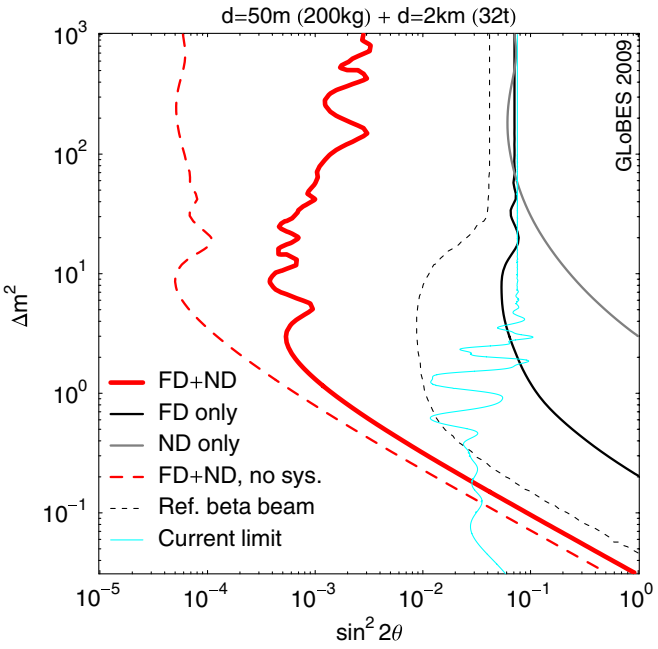

FIG. 5 (color online). Exclusion limit in the $\sin^2 2\theta$-Δm^2 plane for our default configuration including systematics (thick solid curve, 90% C.L., 2 d.o.f.). The thick dashed curve refers to our ideal detectors (no systematics), with near detectors (ND) and far detectors (FD) combined. The thin solid curves illustrate the results for the near (50 m) and far (2 km) detectors if operated separately, but with full systematics. The effects of averaging over the decay straights are taken into account. The thin dashed curve corresponds to the default beta beam setup from Ref. [29] for comparison. The thin gray/cyan curve is the current limit from Bugey [74] and CHOOZ [75] (taken from Ref. [16]).

sion, it should be clear that the results in this case do not depend very much on the actual numbers for the systematical errors. Nevertheless, there is a considerable deviation from the no-systematics case (dashed curve). The improvement towards this hypothetical sensitivity requires a very good understanding of the cross sections at the level of $\sin^2 2\theta$ sensitivity. We have also checked that the performance cannot even be significantly improved with considerably larger detectors, because of the systematics limitation (even without the geometric effect of the beam included).

Figure 5 shows that the sensitivity of a neutrino factory experiment to (V)SBL ν_e disappearance represents a dramatic improvement with respect to the sensitivity of reactor experiments, which is at the level of $\sin^2 2\theta \sim 10^{-1}$ at large values of Δm^2 (cf. thin gray/cyan curve). Moreover, the neutrino factory measurement with the near-far detector setup discussed in Sec. III is model independent, whereas reactor measurements of $P_{\bar{e}\bar{e}}$ depend on the calculated flux of $\bar{\nu}_e$'s produced in a reactor. Reactor neutrino experiments cannot take advantage of the near-far detector approach to get a model-independent result for (V)SBL ν_e disappearance, because for a typical reactor neutrino energy of 1 MeV, the oscillation length corresponding to $\Delta m^2 \approx 10^2$ eV^2 is of the order of 1 cm.

It is interesting to note that the near-far detector setup that we have chosen is sensitive to ν_e disappearance with small mixing ($\sin^2 2\theta \gtrsim 2 \times 10^{-3}$) for values of Δm^2 as large as 10^3 eV. The condition for the observation of a spectral distortion caused by neutrino oscillations is that the uncertainty of the phase of the oscillations due to the energy resolution in Eq. (10) is smaller than about $\pi/2$. One can easily find that this happens for neutrino energies

$$E \gtrsim \left[\frac{\varepsilon \Delta m^2 L_{\text{eff}}}{2\pi E_0^{1/2}}\right]^{2/3}, \tag{16}$$

where we have considered the effective baseline in Eq. (14). Since for the near detector $L_{\text{eff}} \simeq 180$ m, if $\Delta m^2 = 10^3$ eV the condition (16) is satisfied for $E \gtrsim 18$ GeV. Since for the assumed $E_\mu = 25$ GeV the neutrino energy spectrum extends up to 25 GeV, as shown by the curve in Fig. 1 of Ref. [67] with off-axis angle $\theta = 0°$, the oscillations are not completely averaged out in the highest-energy bins. This is illustrated in the left panel of Fig. 4, in which the line corresponding to $\Delta m^2 = 10^3$ eV has the constant averaged value $0.5\sin^2 2\theta - 1 = -0.05$ (for the assumed $\sin^2 2\theta = 0.1$) only for $E \lesssim 10$ GeV. Other curves illustrate the distortion of the event rate spectrum for smaller values of Δm^2. One can see that the lower limit of the sensitivity to Δm^2 of the near detector is about 1 eV^2, which instead produces a strong spectral distortion in the far detector (right panel of Fig. 4).

We also show in Fig. 5 a comparison with the default setup in Ref. [29] (thin dashed curve). This setup uses a low-gamma ($\gamma \simeq 30$) beta beam with inverse beta decay as a detection interaction, which means that it is not surprising that our result is about an order of magnitude better. Compared to Ref. [29], which uses only one detector and therefore runs in the systematics limitation in the larger Δm^2 range, we also have very good sensitivity for large Δm^2. While both approaches rely on near detectors receiving neutrinos from a storage ring, they are conceptually very different: Ref. [29] uses the fact that the inverse beta decay reaction is well known to control systematics, whereas we control the shape error with two sets of detectors in the fashion of the new generation of reactor experiments.

It is interesting to examine not only the sensitivity of our experimental setup to (V)SBL ν_e disappearance, which corresponds to a negative result producing an exclusion curve as in Fig. 5, but also what the results could be if a signal is observed, i.e., if ν_e and $\bar{\nu}_e$ disappear.

In Fig. 6, we show three qualitatively different possible results for the test values of the neutrino oscillation parameters marked by the diamonds. In the left panel, no degenerate solutions are present, and the parameters can be very well measured. There is hardly any effect of the averaging over the decay straights, as one can read off

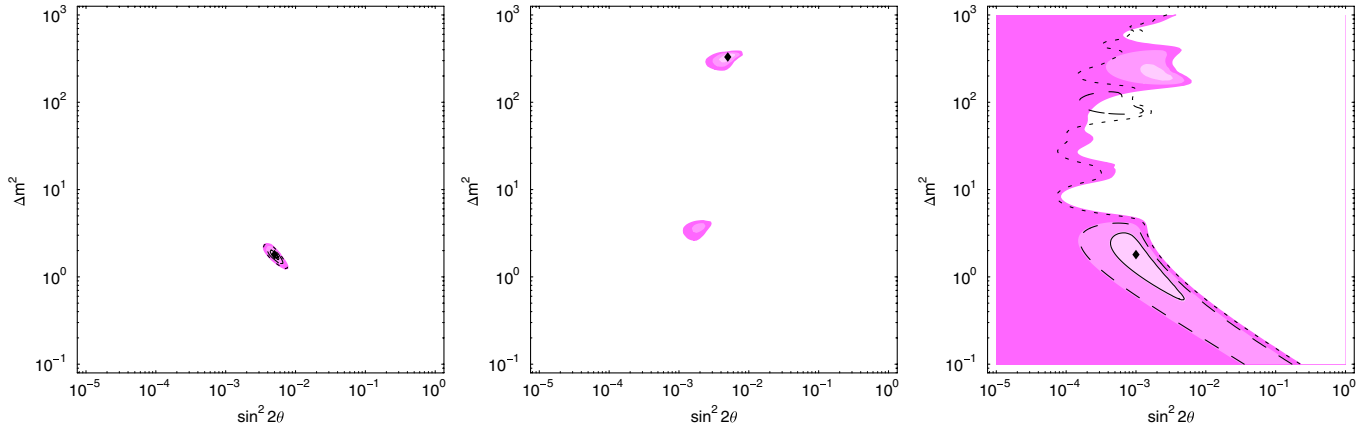

FIG. 6 (color online). Fits in the $\sin^2 2\theta$-Δm^2 plane for three chosen test points marked by the diamonds (1σ, 2σ, 3σ, 2 d.o.f.). Here *CPT* invariance is assumed. Near (50 m) and far (2 km) detectors are used with our systematics model; the effects of averaging over the decay straights are taken into account. The unshaded contours show the result without averaging over the straights. They are too small to be visible in the middle panel.

from the differences between the shaded and unshaded contours, because the far detectors dominate the sensitivity and oscillations have not yet developed at the near detectors. In the middle panel, we still have an excellent measurement dominated by the near detectors. In this case, however, the averaging effects over the straights are very important, and the contours without averaging are hardly visible. In particular, a degenerate solution appears at a smaller Δm^2. In the right panel, we show an even more extreme case, where only at the 2σ confidence level can $\sin^2 2\theta = 0$ be excluded.

V. *CPT* VIOLATION

In this section we discuss the potentiality of the experimental setup described in Fig. 1, with two pairs of near-far detectors, to reveal a violation of *CPT* symmetry, considering the different electron neutrino and antineutrino survival probabilities in Eqs. (2) and (3) as functions of the *CPT* asymmetries in Eq. (5).

Since there are four independent parameters, given by Eqs. (6)–(9), for simplicity we consider three test points inspired by Refs. [16–18]:

$$\text{T1: } \sin^2 2\theta = 0.05, \qquad \Delta m^2 = 1.8 \text{ eV}^2, \tag{17}$$

$$\text{T2: } \sin^2 2\theta = 0.1, \qquad \Delta m^2 = 20 \text{ eV}^2, \tag{18}$$

$$\text{T3: } \sin^2 2\theta = 0.1, \qquad \Delta m^2 = 330 \text{ eV}^2, \tag{19}$$

and $a_{CPT} = m_{CPT} = 0$. We fit the corresponding simulated data, allowing for nonzero values of a_{CPT} and m_{CPT} in order to explore the sensitivity to the measurement of these parameters.

Test point T1 is motivated by the best fit of the data of the Bugey SBL reactor experiment [74], which is compatible with the data of the Chooz reactor experiment [75] and the neutrino oscillation explanation of the Gallium anomaly [16]. Test points T2 and T3 are motivated by a possible explanation of the MiniBooNE low-energy anomaly through VSBL ν_e disappearance, which is compatible with the neutrino oscillation explanation of the Gallium anomaly [17,18]. Even if values of Δm^2 larger than about 1 eV^2 are incompatible with the existing standard cosmological bound on the sum of neutrino masses [9,76], we think that it is wise to test such bounds in laboratory experiments. A violation of the bound may lead to the discovery of fundamental new physics related to nonstandard cosmological effects.

The best-fit regions for the three test points are shown in Fig. 7. The dashed curves represent the results without taking into account the averaging over the decay straights. Test point T1 (upper row), with a relatively small Δm^2, is dominated by the far detectors, whereas in the near detectors (almost) no oscillations are present. Therefore, the cross sections can be directly reconstructed from the near detectors, and the fits are very clean. The effects of averaging over the straights are small because the signal is in the far detectors, which sees a point source. The oscillation parameters can be measured at the level of 2% (1σ), and the *CPT* invariance can be constrained at the same level.

Test point T3 (lower row of Fig. 7) is dominated by the short baseline, which means that the averaging effects over the straights are very important. The longer baseline measures the product of cross sections and $1 - 0.5\sin^2 2\theta$, which means that Δm^2 can, before the averaging over the straights (dashed curves), be very well measured compared to the mixing angle since it remains as a net effect between the two detectors. Only after the averaging effects can both oscillation parameters be measured at the level of 1% (1σ), and the *CPT* invariance can be constrained at a similar level.

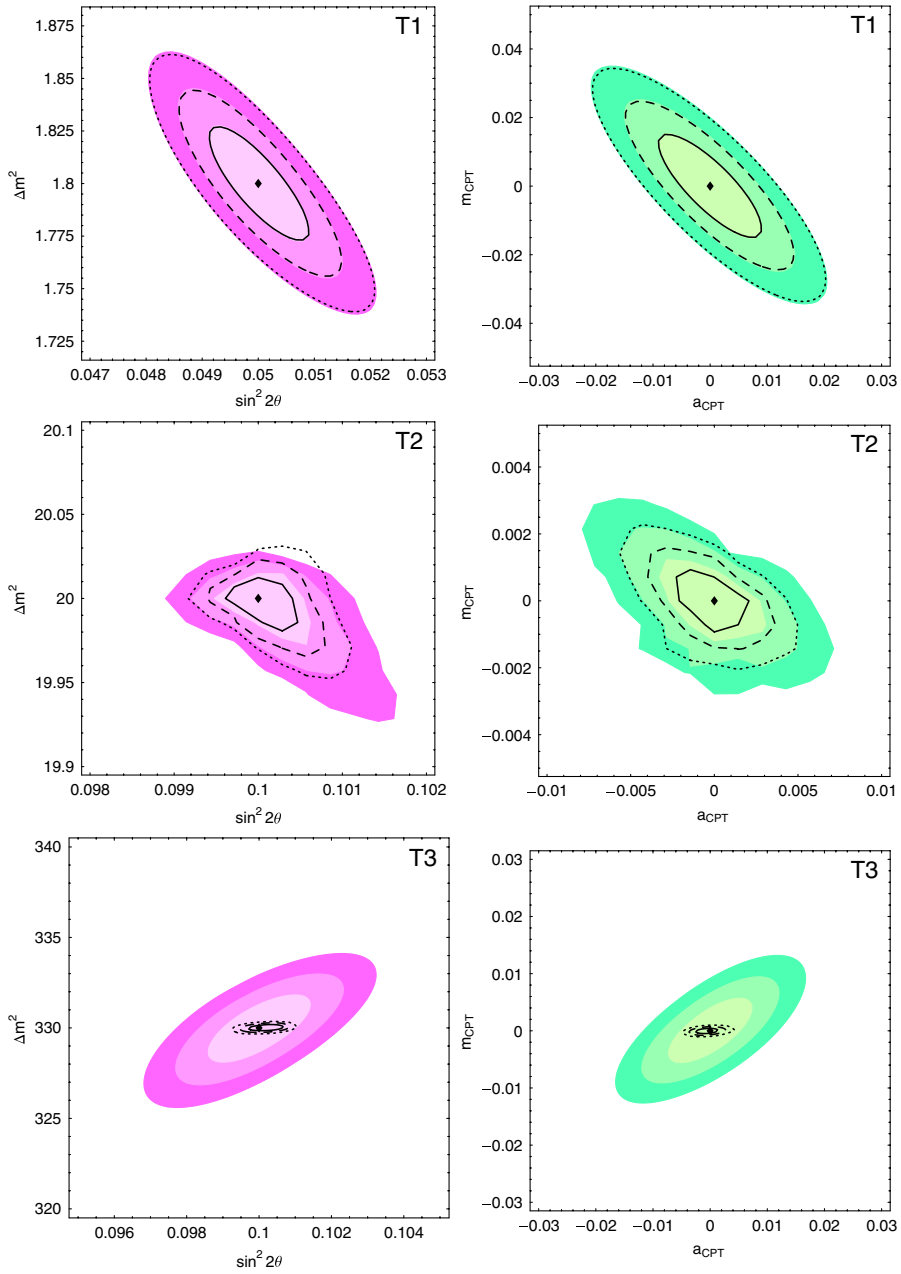

FIG. 7 (color online). Best-fit regions in the Δm^2-$\sin^2 2\theta$ and a_{CPT}-m_{CPT} planes for the test points defined in the main text (1σ, 2σ, 3σ, 2 d.o.f.). Note that different baselines were chosen for the test points. The dashed curves represent the results without taking into account the averaging over the decay straights.

Test point T2 (middle row of Fig. 7) shows a complicated case with an intricate interplay between systematics and oscillation parameter correlations. Since there is an oscillation effect in both baselines, this case does not correspond to a classical near-far detector combination. The *a priori* excellent precisions for the oscillation parameters are spoilt by some complicated correlations. Nevertheless, percent level precisions are possible.

Instead of constraining *CPT* invariance, we can also discuss the discovery reach for *CPT* violation. In this case, we assume that nature has implemented a small (positive) a_{CPT} or m_{CPT}, and we fit the simulated data with the fixed parameters $a_{CPT} = m_{CPT} = 0$ (corresponding to *CPT* invariance), while we marginalize over the oscillation parameters $\sin^2 2\theta$ and Δm^2. We show in Fig. 8 the discovery reach for *CPT* violation from a_{CPT} (left panel) or m_{CPT} (right panel) as a function of the true $\sin^2 2\theta$ and true Δm^2. The different contours indicate for how small (true) values of $a_{CPT} > 0$ (left panel) or $m_{CPT} > 0$ (right panel) *CPT* violation will be discovered at the 3σ

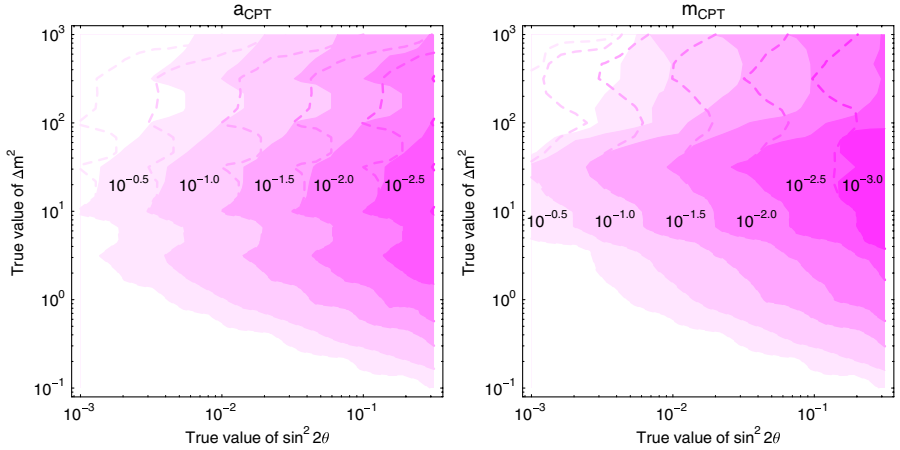

FIG. 8 (color online). Discovery reach for CPT violation from a_{CPT} (left panel) or m_{CPT} (right panel) as a function of the true $\sin^2 2\theta$ and true Δm^2. The different contours indicate for how small (true) values of $a_{CPT} > 0$ (left panel) or $m_{CPT} > 0$ (right panel) CPT violation will be discovered at the 3σ confidence level, as labeled at the contours. The dashed curves show the result if the averaging over the decay straights is not taken into account.

confidence level, as labeled at the contours. The dashed curves show the result if the averaging over the decay straights is not taken into account.

From Fig. 8, CPT violation may be discovered even if it is as small as 10^{-3}, provided that $\sin^2 2\theta$ is large enough. However, even for very small $\sin^2 2\theta$, a CPT violation of order unity is testable with our setup. Note that for larger Δm^2 and especially for m_{CPT}, the averaging over the decay straights strongly reduces the performance (by about 1 order of magnitude).

In Ref. [18], a difference of $A_{ee}^{CPT} \equiv P_{ee} - P_{\bar{e}\bar{e}} = -0.17^{+0.09}_{-0.07}$ at 90% C.L. was identified as the asymmetry between the electron neutrino and antineutrino VSBL disappearance probabilities, which can explain the Gallium radioactive source experiments anomaly [14] and the MiniBooNE low-energy anomaly [13] without conflicting with the absence of $\bar{\nu}_e$ disappearance in reactor neutrino experiments (see Ref. [77]). It is interesting to investigate if such CPT violation can be measured in a neutrino factory experiment with the near-far pairs of detectors that we have considered so far.

Since in Ref. [18] Δm^2 was considered to be large, in the range

$$20\ \text{eV}^2 \lesssim \Delta m^2 \lesssim 330\ \text{eV}^2, \tag{20}$$

the neutrino and antineutrino survival probabilities were assumed to be averaged, leading to $A_{ee}^{CPT} = 0.5(\sin^2 2\theta_{\bar{\nu}} - \sin^2 2\theta_{\nu})$. In this case, the asymmetry a_{CPT} is given by

$$a_{CPT} = \frac{1}{4\theta} \arcsin\left(\frac{-2A_{ee}^{\text{CPT}}}{\sin 4\theta}\right). \tag{21}$$

Since $|a_{CPT}| \leq 1$, the mixing angle has a lower limit which depends on the value of A_{ee}^{CPT}. Moreover, since $|\sin 4\theta| \leq 1$ and $\theta \leq \pi/2$, $|a_{CPT}|$ also has a lower limit, plotted in Fig. 9 for $A_{ee}^{CPT} < -0.08$, which is the 95% C.L. limit found in Ref. [18]. One can see that the bound on A_{ee}^{CPT} implies that $\sin^2 2\theta \gtrsim 4 \times 10^{-2}$ and $|a_{CPT}| \gtrsim 0.10$. Confronting these values with the left panel in Fig. 8, and taking into account the fact that we consider the large values of Δm^2 in the range (20), it is clear that the CPT violation required by $A_{ee}^{CPT} \lesssim -0.08$ will be easily discovered in a neutrino factory experiment with the near-far pairs of detectors that we have considered.

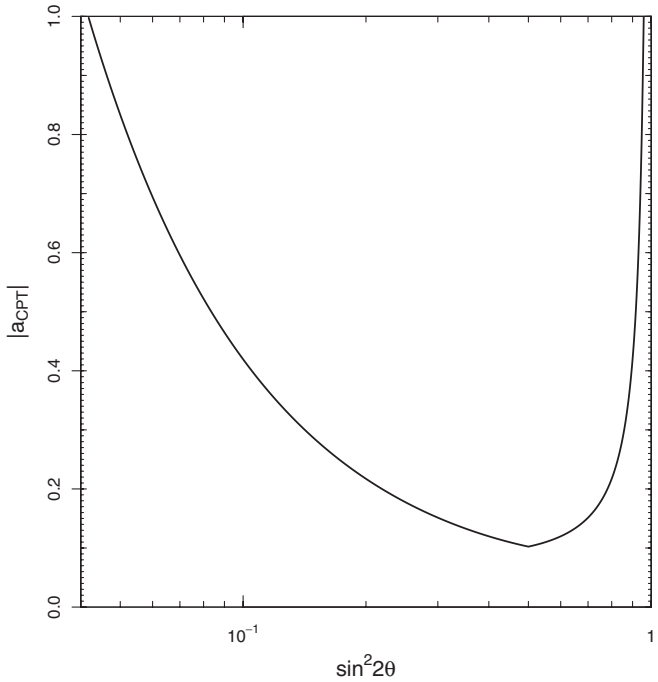

FIG. 9. Lower limit for $|a_{CPT}|$ obtained from Eq. (21) with $A_{ee}^{CPT} < -0.08$, which is the 95% C.L. limit found in Ref. [18].

VI. SUMMARY AND CONCLUSIONS

In this work we have discussed the potentiality of testing SBL (with $10^{-1} \lesssim \Delta m^2_{\mathrm{SBL}} \lesssim 10\ \mathrm{eV}^2$) and VSBL (with $10 \lesssim \Delta m^2_{\mathrm{VSBL}} \lesssim 10^3\ \mathrm{eV}^2$) electron neutrino disappearance in a neutrino factory experiment, based on the current setup of the International Design Study for the Neutrino Factory [63]. Since this setup uses both muon and antimuon decays, a possible difference between the neutrino and antineutrino disappearance can be studied, which could constitute a revolutionary discovery of *CPT* violation.

We showed that for these purposes the ideal configuration would be two pairs of near-far detectors (shown in Fig. 1), in a similar fashion to reactor experiments with near and far detectors (Double Chooz [70], Daya-Bay [71], etc.), to cancel systematics. The near detectors are chosen to be at a distance of about 50 m from the muon storage ring, in order to be sensitive to oscillations due to a Δm^2 as large as about $10^3\ \mathrm{eV}^2$. For the far detectors an appropriate distance from the muon storage ring is about 2 km, which gives a good sensitivity to oscillations generated by a Δm^2 as small as about $10^{-1}\ \mathrm{eV}^2$. In this way, it is possible to explore (V)SBL ν_e and $\bar{\nu}_e$ disappearance with effective oscillation amplitude $\sin^2 2\theta$ as small as about 10^{-3} for $\Delta m^2 \gtrsim 1\ \mathrm{eV}^2$ (see Fig. 5), taking advantage of the comparison of the event rates measured in the near and far detectors, which reduces dramatically the systematic uncertainties due to insufficient knowledge of the cross sections (see the discussion in Sec. III).

We have also shown, in Sec. V, that the chosen detector setup provides a good sensitivity to the measurement of a difference of the rates of ν_e and $\bar{\nu}_e$ disappearance which would be a signal of *CPT* violation. For instance, our setup is sensitive to an asymmetry between the neutrino and antineutrino mass squared differences at the level of up to 10^{-3}, depending on the value of the mixing angle. Let us emphasize that a discovery of *CPT* violation would represent a revolution in our knowledge of fundamental physics, because the *CPT* symmetry is a fundamental symmetry of local relativistic quantum field theory. Therefore, pursuing this line of investigation is of fundamental importance.

ACKNOWLEDGMENTS

We would like to thank Sanjib Agarwalla for providing the beta beam reference curve in Fig. 5, and Patrick Huber for useful discussions. This work was supported by the European Union under the European Commission Framework Programme 07 Design Study EUROnu, Project No. 212372. W. Winter also would like to acknowledge support from the Emmy Noether program of Deutsche Forschungsgemeinschaft. C. Giunti would like to thank the Department of Theoretical Physics of the University of Torino for hospitality and support.

[1] S. M. Bilenky, C. Giunti, and W. Grimus, Prog. Part. Nucl. Phys. **43**, 1 (1999).
[2] M. Gonzalez-Garcia and Y. Nir, Rev. Mod. Phys. **75**, 345 (2003).
[3] C. Giunti and M. Laveder, arXiv:hep-ph/0310238; in *Developments in Quantum Physics–2004*, edited by F. Columbus and V. Krasnoholovets (Nova Science Publishers, Hauppauge, NY, 2004), pp. 197–254.
[4] M. Maltoni *et al.*, New J. Phys. **6**, 122 (2004).
[5] G. L. Fogli *et al.*, Prog. Part. Nucl. Phys. **57**, 742 (2006).
[6] A. Strumia and F. Vissani, arXiv:hep-ph/0606054.
[7] C. Giunti and C. W. Kim, *Fundamentals of Neutrino Physics and Astrophysics* (Oxford University Press, New York, 2007).
[8] M. C. Gonzalez-Garcia and M. Maltoni, Phys. Rep. **460**, 1 (2008).
[9] G. L. Fogli *et al.*, Phys. Rev. D **78**, 033010 (2008).
[10] T. Schwetz, M. Tortola, and J. W. F. Valle, New J. Phys. **10**, 113011 (2008).
[11] A. Aguilar *et al.* (LSND Collaboration), Phys. Rev. D **64**, 112007 (2001).
[12] B. Armbruster *et al.* (KARMEN Collaboration), Phys. Rev. D **65**, 112001 (2002).
[13] A. A. Aguilar-Arevalo (MiniBooNE Collaboration), Phys. Rev. Lett. **102**, 101802 (2009).
[14] J. N. Abdurashitov *et al.* (SAGE Collaboration), Phys. Rev. C **80**, 015807 (2009).
[15] C. Giunti and M. Laveder, Mod. Phys. Lett. A **22**, 2499 (2007).
[16] M. A. Acero, C. Giunti, and M. Laveder, Phys. Rev. D **78**, 073009 (2008).
[17] C. Giunti and M. Laveder, Phys. Rev. D **77**, 093002 (2008).
[18] C. Giunti and M. Laveder, Phys. Rev. D **80**, 013005 (2009).
[19] M. Sorel, J. Conrad, and M. Shaevitz, Phys. Rev. D **70**, 073004 (2004).
[20] G. Karagiorgi *et al.*, arXiv:0906.1997 [Phys. Rev. D (to be published)].
[21] G. Karagiorgi *et al.*, Phys. Rev. D **75**, 013011 (2007).
[22] C. Grieb, J. Link, and R. S. Raghavan, Phys. Rev. D **75**, 093006 (2007).
[23] D. C. Latimer, J. Escamilla, and D. J. Ernst, Phys. Rev. C **75**, 042501 (2007).
[24] A. Donini *et al.*, J. High Energy Phys. 12 (2007) 013.
[25] M. Maltoni and T. Schwetz, Phys. Rev. D **76**, 093005 (2007).
[26] S. Goswami and W. Rodejohann, J. High Energy Phys. 10 (2007) 073.
[27] A. Bandyopadhyay and S. Choubey, arXiv:0707.2481.

[28] T. Schwetz, J. High Energy Phys. 02 (2008) 011.
[29] S. K. Agarwalla, P. Huber, and J. M. Link, arXiv: 0907.3145.
[30] R. L. Awasthi and S. Choubey, Phys. Rev. D **76**, 113002 (2007).
[31] S. Choubey, J. High Energy Phys. 12 (2007) 014.
[32] D. Boyanovsky, H. J. de Vega, and N. Sanchez, Phys. Rev. D **77**, 043518 (2008).
[33] G. Gentile, H. S. Zhao, and B. Famaey, arXiv:0712.1816.
[34] G. W. Angus, arXiv:0805.4014.
[35] A. Donini and O. Yasuda, arXiv:0806.3029.
[36] O. Civitarese and M. E. Mosquera, Phys. Rev. C **77**, 045806 (2008).
[37] A. Melchiorri *et al.*, J. Cosmol. Astropart. Phys. 01 (2009) 036.
[38] M. A. Acero and J. Lesgourgues, Phys. Rev. D **79**, 045026 (2009).
[39] O. W. Greenberg, Found. Phys. **36**, 1535 (2006).
[40] O. W. Greenberg, Phys. Rev. Lett. **89**, 231602 (2002).
[41] G. Barenboim *et al.*, Phys. Lett. B **537**, 227 (2002).
[42] V. A. Kostelecky and N. Russell, arXiv:0801.0287.
[43] H. Murayama and T. Yanagida, Phys. Lett. B **520**, 263 (2001).
[44] G. Barenboim *et al.*, J. High Energy Phys. 10 (2002) 001.
[45] S. M. Bilenky *et al.*, Phys. Rev. D **65**, 073024 (2002).
[46] G. Barenboim, L. Borissov, and J. Lykken, Phys. Lett. B **534**, 106 (2002).
[47] A. Strumia, Phys. Lett. B **539**, 91 (2002).
[48] J. N. Bahcall, V. Barger, and D. Marfatia, Phys. Lett. B **534**, 120 (2002).
[49] H. Murayama, Phys. Lett. B **597**, 73 (2004).
[50] V. Barger, D. Marfatia, and K. Whisnant, Phys. Lett. B **576**, 303 (2003).
[51] H. Minakata and S. Uchinami, Phys. Rev. D **72**, 105007 (2005).
[52] M. C. Gonzalez-Garcia, M. Maltoni, and T. Schwetz, Phys. Rev. D **68**, 053007 (2003).
[53] S. Antusch and E. Fernandez-Martinez, Phys. Lett. B **665**, 190 (2008).
[54] A. D. Dolgov, arXiv:0903.4318.
[55] J. Evans, MINOS (2009), HEP 2009, *The 2009 Europhysics Conference on High Energy Physics, 2009, Krakow, Poland*; http://indico.ifj.edu.pl/MaKaC/contributionDisplay.py?contribId=671\&sessionId=8\&confId=11.
[56] G. Barenboim and J. D. Lykken, arXiv:0908.2993.
[57] V. A. Kostelecky and M. Mewes, Phys. Rev. D **69**, 016005 (2004).
[58] D. Hooper, D. Morgan, and E. Winstanley, Phys. Rev. D **72**, 065009 (2005).
[59] T. Katori, V. A. Kostelecky, and R. Tayloe, Phys. Rev. D **74**, 105009 (2006).
[60] S. Hollenberg, O. Micu, and H. Pas, arXiv:0906.5072 [Phys. Rev. D (to be published)].
[61] S. Esposito and G. Salesi, arXiv:0906.5542.
[62] J. L. B. Alba *et al.*, arXiv:0907.1979.
[63] International Design Study of the Neutrino Factory, http://www.ids-nf.org.
[64] T. Abe *et al.* (ISS Detector Working Group), JINST **4**, T05001 (2009).
[65] S. Geer, O. Mena, and S. Pascoli, Phys. Rev. D **75**, 093001 (2007).
[66] A. Bross *et al.*, Phys. Rev. D **77**, 093012 (2008).
[67] J. Tang and W. Winter, Phys. Rev. D **80**, 053001 (2009).
[68] P. Huber, M. Lindner, and W. Winter, Comput. Phys. Commun. **167**, 195 (2005).
[69] P. Huber *et al.*, Comput. Phys. Commun. **177**, 432 (2007).
[70] F. Ardellier *et al.* (Double Chooz Collaboration), arXiv: hep-ex/0606025.
[71] X. Guo *et al.* (Daya-Bay Collaboration), arXiv:hep-ex/0701029.
[72] P. Huber *et al.*, Nucl. Phys. **B665**, 487 (2003).
[73] P. Huber *et al.*, J. High Energy Phys. 05 (2006) 072.
[74] B. Achkar *et al.*, Nucl. Phys. **B434**, 503 (1995).
[75] M. Apollonio *et al.* (CHOOZ Collaboration), Eur. Phys. J. C **27**, 331 (2003).
[76] F. De Bernardis *et al.*, Phys. Rev. D **78**, 083535 (2008).
[77] C. Bemporad, G. Gratta, and P. Vogel, Rev. Mod. Phys. **74**, 297 (2002).